11A.7 LIGHTNING INITIATION AND INTENSITY NOWCASTING BASED ON ISOTHERMAL RADAR REFLECTIVITY — A CONCEPTUAL MODEL

Linus H.Y. Yeung*[1], Edwin S.T. Lai[1] and Samson K.S. Chiu[2]
[1] Hong Kong Observatory, Hong Kong, China
[2] City University of Hong Kong, Hong Kong, China

1. INTRODUCTION

Intense convective activity associated with summer monsoon, monsoon troughs and tropical cyclones poses a major weather threat in the warm seasons of Hong Kong. Very often, such intense convective activity will also trigger other types of hazardous weathers. As shown in Table I, lightning strikes, heavy rainstorms, damaging downbursts/squalls, hails, waterspouts and even tornadoes are not uncommon in Hong Kong. In terms of occurrence frequencies as shown in Table I, thunderstorm lightning is actually the most frequent type of weather hazard in Hong Kong. At the Hong Kong Observatory (HKO), a second generation nowcasting system is currently under development to track and nowcast such severe weather phenomena. For more details on SWIRLS (Short-range Warning of Intense Rainstorms in Localized Systems), readers are referred to Li and Lai 2004.

In this paper, a radar-based scheme for the nowcasting of lightning initiation and intensity is presented. In Section 2, the simple conceptual model behind the scheme is outlined. The selection of key radar parameters as lightning predictors and the considerations involved are given in Section 3. The importance of near-storm thermal structure and the corresponding derivation of isothermal radar reflectivities are highlighted in Section 4. The details of the lightning nowcast scheme are documented in Section 5 and the preliminary testing results presented in Section 6. Conclusions and further improvement areas are discussed in Section 7.

Table I – Occurrence frequencies of various types of weather hazards in the warm seasons of Hong Kong.

Weather Hazards	Period	Total Number
Thunder/Lighting	1977-2006	2620 warnings
Amber Rainstorm(1)	1997-2006	240 warnings
Red Rainstorm(1)	1997-2006	48 warnings
Black Rainstorm(1)	1997-2006	13 warnings
Severe Squalls(2)	1987-2006	214 days
Hail	1977-2006	30 reports
Waterspout	1977-2006	22 reports
Tornado	1982-2006	8 reports

Note: (1) Amber, Red and Black Rainstorms respectively refer to hourly rainfall ≥ 30, 50 and 70 mm widespread over Hong Kong. (2) Severe squalls is operationally defined as 1-sec wind speed ≥ 70 km/h (near surface).

2. CONCEPTUAL MODEL

Following Zajac and Weaver's extension (Zajac & Weaver 2002) to the classical thunderstorm lifecycle of Byers and Braham (1949), we assume a lightning initiation process through the 4-stage evolution sequence as shown in Table II.

Symbols ⇑ and ⇓ in Table II represent updraft and downdraft in a convective cloud, whereas ←→ and →← imply divergence and convergence respectively. Hydrometeors critical to cumulus cloud electrification, namely cloud liquid water, supercooled cloud liquid water, ice crystal and graupel, are denoted by symbols 💧, 💧, *, and △ respectively. Positive and negative charges are presented by symbols ⊕ and ⊖. Positive and negative ground strikes are symbolized as ⚡ and ⚡. The symbol ▽ has its usual meaning of shower. The relative sizes of these symbols are drawn to contrast their relative abundance/magnitude.

Though simplistic, the conceptual model in Table II captures the essence of recent studies on cloud electrification, namely: (i) the formation of graupel at sub-zero levels and its correlation to initial electrification (Dye *et al* 1986); (ii) charges generated by graupel-ice collision under strong convection; (iii) charges separated vertically by updrafts and downdrafts resulting in a large-scale electrical dipole structure in a mature thundercloud, with positive charges on the lighter ice crystals floating mainly near the cloud top and negative charges on the heavier graupel tumbling mainly towards the lower portion of a thundercloud (Williams 1985); (iii)

Table II – Summary of the conceptual model for lightning initiation.

Isothermal Layers	(i) Shallow Cu			(ii) Towering Cu			(iii) mature Cb			(iv) decaying Cb		
	D	H	E	D	H	E	D	H	E	D	H	E
below –40°C							⇑	*	⊕	⇑	*	⊕
–20 to –40°C				⇑	*	⊕	⇑	*	⊕	⇑	*	
–10 to –20°C	⇑	*		⇑⇓	* △	⊖	⇑⇓	* △	⊖		*	
0 to –10°C	⇑	💧		⇑	* 💧		⇑⇓	* △ 💧	⊖		*	
above 0°C	⇑	💧		⇑	💧		⇑⇓	△ 💧	⊖	⇓	△	
near surface	→←			→←	▽		←→	▽	⚡	←→	▽	⚡

Note : Headings D, H and E stand for vertical dynamics, hydrometeors and electric charges respectively. Other symbols are explained in the main text of Section 2.

* *Corresponding author address*: Linus H.Y. Yeung, Hong Kong Observatory, 134A, Nathan Road, Kowloon, Hong Kong, China; e-mail: hyyeung@hko.gov.hk

locations of charge centres being governed by vertical temperature profile rather than height, with the main negative charge centre residing in the mixed-phase layer between –5 to –25°C (Mason 1953; Moore & Vonnegut 1977; Jayaratne 2003); (iv) cloud-to-ground (CG) lightning initiated in the mixed-phase layer. In the present conceptual model, it is further assumed that the first CG lightning from a thunderstorm cell is usually associated with its main precipitation shaft (radar reflectivity ≥ 25 dBZ).

Some studies (e.g. Williams 1989) showed that a small pocket of positive charges associated with the precipitation shaft exists below the main negative centre, close to the freezing level. To a first order approximation, we ignore the small positive pocket and assume the majority of initial CG strikes are originated from the main negative centre of the large-scale dipole. Actual lightning observation in our domain also supported this assumption. Positive CG lightning from anvil does happen. To simplify the conceptual model on CG lightning initiation, we assume positive strikes mainly occur in the dissipating stage of a cumulonimbus.

3. LIGHTNING PREDICTORS

Based on the above conceptual model, the precursors for CG lightning initiation are identified with the following signatures: (a) high radar reflectivity values in the mixed-phase layer indicating the presence of graupel and hence the abundance of negative charge carriers; (b) high radar echo top (denoted as TOP) indicating strong updraft and vertical separation of charges; and (c) high value of vertically integrated liquid (denoted as VIL) indicating an abundant supply of cloud water for ice and graupel formation and riming.

To quantify signature (a), the radar reflectivity at three isotherms, namely 0, –10 and –20°C, are chosen as representative parameters and denoted as REF_0, REF_{-10}, REF_{-20} respectively. To retrieve radar reflectivity on these isothermal layers, the temperature structure of the atmosphere at the retrieval time is required. For this purpose, the 3-dimensional temperature analysis information from an hourly-updated Local Analysis and Prediction System (LAPS) (Albers *et al.* 1996) is used. The data processing technique is given in more detail in Section 4 below. For signature (b), TOP is defined as the height of the 10-dBZ iso-surface ceiling. Regarding signature (c), VIL is calculated from 1 to 18 km. Similar radar parameters were also adopted as lightning predictors in previous lightning nowcast studies (e.g. Gremillion & Orville 1999, Lakshmanan & Stumpf 2005).

To fill the cone of silence in a radar volume scan, the above radar products are generated from a mosaic of two S-band Doppler weather radars in Hong Kong. The radars are located on two hill tops, namely Tai Mo Shan (TMS) and Tate's Cairn (TCR), about 11 km apart. Fig. 1 shows the radarscope centred at TMS out to 150 km range, with the locations of the two Doppler radars marked by cyan squares. TMS and TCR radars are time synchronized, providing full volume scan data every 6 minutes with a fixed scanning schedule at 00, 06, 12, …, 54 minute of the hour. In composing a radar mosaic, the maximum reflectivity value between the two radars is taken at co-located points.

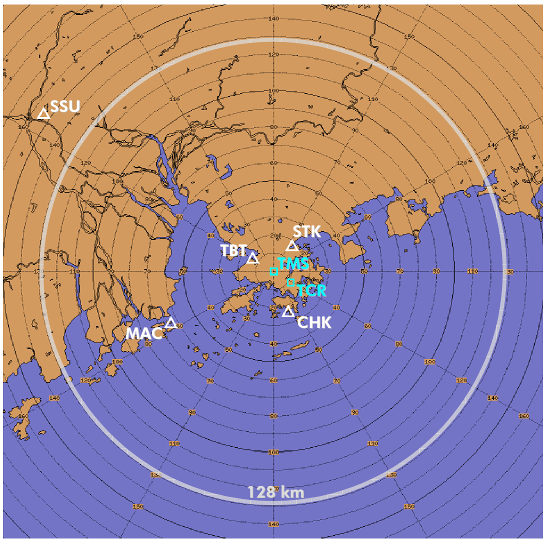

Fig. 1 Radarscope of Hong Kong out to the 150 km range. Concentric rings indicate horizontal range in intervals of 10 km. Circle in light gray indicates the 128-km radarscope range. Locations of Doppler radars marked by cyan squares and LLIS sensors by white triangles. The three-letter codes refer to the names of the various sensor sites (see main text in Section 3).

The lightning data are provided by the Lightning Location Information System (LLIS) of HKO. LLIS has been in operation since June 2005, providing real-time lightning strike information, including lightning stroke time, 2-dimensional location (latitude and longitude), confidence ellipse, stroke type (cloud or ground), polarity, peak current, and rise/fall times of current waveform. Under the current network configuration, LLIS has 5 IMPACT ESP sensors (Vaisala 2004), with 3 located at Tsim Bei Tsui (TBT), Sha Tau Kok (STK) and Chung Hum Kok (CHK) of Hong Kong, 1 in Macau (MAC) and 1 in San Shui (SSU) of Guangdong. Sensor sites are marked by white triangles in Fig. 1. The algorithm for locating lightning is based on a combined magnetic-direction-finding and time-of-arrival method (Cummins *et al.* 1998). Generally speaking, the location accuracy (LA) of CG lightning detected by LLIS is about 500 m within the sensor network and decreases progressively to about 4000 m on the east and southeastern rim of the 128-km radarscope. In terms of detection efficiency (DE), it is generally above 90% within the sensor network and about 80-90% elsewhere inside the 128-km radarscope. For cloud-to-cloud lightning, both LA and DE are considerably less.

4. ISOTHERMAL RADAR REFLECTIVITY

To retrieve radar reflectivity on a given constant temperature surface, we need to know the height field of such an iso-surface. To prepare this in real-time, the 3-dimensional temperature analysis information from LAPS is used. At HKO, LAPS analysis is performed every 60 minutes on the hour, ingesting various available observations including conventional synoptic observations (surface and upper-air), automatic weather station data, wind profiler data, geostationary satellite data and Doppler radar data. Currently, the background fields are prepared from the short-range forecast data of the Operational Regional Spectral Model (JMA 2002) of HKO.

Using the 3-D temperature and geopotential height fields of LAPS output, a 2-D altitude field of a given isotherm is generated on the LAPS grid (5-km resolution, in Mercator projection) by linear interpolation. From the verification results (unpublished) based on the data sets of May-June 2005, the RMS errors of LAPS temperature analysis were verified (against the 00 and 12 UTC sounding data of Hong Kong and nearby upper-air stations in Guangdong) to be generally less than 2 degrees in mid levels. Next, the altitude of a given isotherm at each point *P* on the radar grid (average spacing of 0.5 km, in azimuthal equidistant projection) is determined by linear interpolation from the altitude values at the 4 nearest LAPS grid points surrounding *P*. For the present study, altitude fields between two consecutive hours are interpolated linearly in time at 6-minute intervals.

With the altitude field of a given isotherm, the corresponding isothermal reflectivity is then obtained by linear interpolation from radar reflectivity at constant height (1-15 km CAPPI products are used).

5. LIGHTNING NOWCAST ALGORITHM

There are three main procedures in our lightning nowcast study: (i) thunderstorm cell identification from radar data, (ii) deriving radar signatures leading up to lightning initiation, and (iii) investigating the correlation between lightning intensity and radar parameters.

5.1 *Thunderstorm Cell Identification*

Storm cells are first identified from the 3-km CAPPI data as contiguous areas of pixels greater than or equal to a prescribed reflectivity threshold. To allow early tracking of storm cells with lightning potential, a relatively low threshold value of 25 dBZ is adopted. A minimum size of 16 pixels is imposed. After identification, ellipses are fit to the cells to represent their geometric properties, including centre location, lengths of semi-major and minor axes, orientation, etc. The detailed procedures are the same as the GTrack algorithm in SWIRLS (Li and Lai 2004). For each storm cell, statistics on the distributions of TOP, VIL, REF_0, REF_{-10}, REF_{-20}, are also calculated and recorded. Amongst the various statistics calculated, the average of the top 10 values in a distribution is used as lightning predictor. In subsequent discussions involving the 5 radar parameters, such top-10 averaged values are implied.

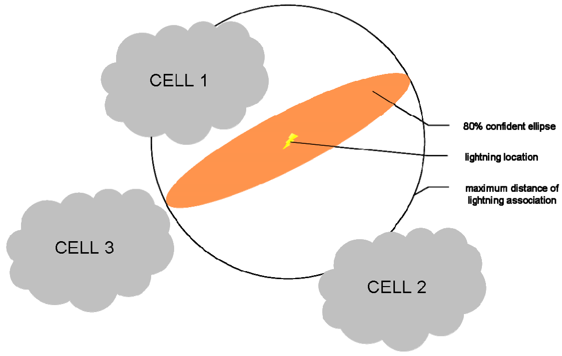

Fig. 2 Association of a lightning strike (yellow symbol at the middle of the oval) with nearby storm cells (gray shadings). The orange oval represents the 80% confidence ellipse of a lightning location as reported by LLIS. The dark circle inscribing the confidence ellipse is taken as the acceptance range for precipitation-shaft lightning. In this illustration, cell 1 rather than cell 2 or 3 is matched with the lightning stroke for its proximity.

5.2 *Lightning Stroke - Storm Cell Association*

Before the relationships between lightning and storm-cell properties can be studied, we need to address the basic question of which observed lightning strokes are associated with which storm cells. This is non-trivial as a significant portion of reported lightning locations are outside the radar footprint of storm cells. To answer this question in an objective way, we first group lightning strokes in batches of 6 minutes in accordance with the radar scanning schedule. Within a batch, the association of lightning strokes with storm cells is mainly based on distance separation. In general, a lightning stroke is assigned to the closest storm cell. When two or more cells are found equally close to a stroke location, the lightning is randomly assigned to one of the equidistant cells.

Since the Thunderstorm Warning in Hong Kong is primarily concerned with ground strikes, only CG lightning data are included in the present study. As explained in Section 2, the initial CG lightning is assumed to be associated with precipitation cores of storm cells. As such, an acceptance range is arbitrarily set to discriminate whether or not a lightning stroke is associated with precipitation core and included in the subsequent analysis. In the present study, the major axis of the 80% confidence ellipse of a CG stroke location is taken as the acceptance range (dark circle in Fig. 2).

The number of CG lightning strokes in 6 minutes assigned to a storm cell through the above procedures is conveniently referred to as cell lightning activity, denoted by symbol α.

5.3 *Lightning Initiation Prediction*

As noted from the scatter plots (a)-(e) shown in Fig.3, cell lightning activity is low when the 5 radar parameters associated with a storm cell are small but soars exponentially when they become large. Based on

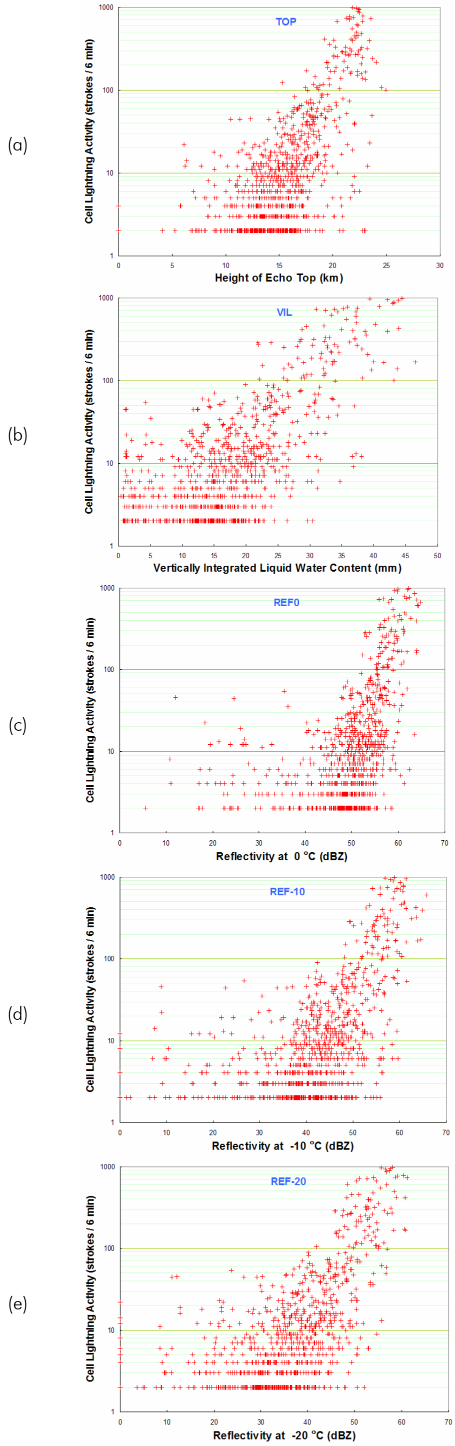

Fig.3 Scatter plots of storm cell CG lightning activity versus the 5 selected radar parameters of storm cells: (a) TOP; (b) VIL; (c) REF_0; (d) REF_{-10}; and (e) REF_{-20}.

such an observation, we model CG lightning initiation as an on-off process: initiation is assumed to occur when the 5 radar parameters exceed a certain set of threshold values.

To find out the possible sets of threshold values for CG lightning initiation, we selected a set of 14 storm cells from July to September 2005 with known CG lightning occurrence and tracked their motions and radar parameters throughout their entire lifecycles. To achieve accurate and consistent results, the tracking was done manually. Since all the 14 storm cells were known to produce CG lightning, every set of radar parameter values preceding their first CG strikes constitutes a candidate set of threshold values for CG lightning initiation. A total of 86 candidate threshold sets were obtained. These data sets are referred to as the Training Data Set.

Next, another data set consisting of 21 independent storm cells with and without CG lightning was selected. This is referred to as the Testing Data Set. Each of the 86 candidate threshold sets was applied in succession to all the 21 storm cells in the Testing Data Set. CG lightning initiation prediction for each of the testing storms was verified against their known cell lightning activity. In this way, the statistics of initiation nowcast performance, including probability of detection (POD), false alarm ratio (FAR), critical success index (CSI) and forecast lead time (LeT), were calculated and the results recorded. Naturally, different candidate threshold sets score differently in skill and lead time but no single set could serve the two purposes simultaneously. The choice of optimal threshold set is therefore a matter of application. Section 6 below presents two optimal threshold sets, one maximizing skill and one maximizing lead time.

5.4 Lightning Intensity Prediction

From Fig.3, it is evident from the higher end of the distributions that linear relationships do exist between the dependent and independent variables. With such observations, we define a dimensionless cell lightning intensity measure, ζ, as the logarithm of α:

$$\zeta = \log_{10}(\alpha) \qquad (1)$$

and proposed a linear relationship between cell lightning intensity and radar parameters as follows

$$\zeta = a + \sum b_i \cdot x_i \qquad (2)$$

where a is a constant, x_i are radar parameters and b_i are correlation coefficients to be found by multiple linear regression method.

The regression analysis showed that TOP, VIL and isothermal REF when expressed in their natural units (i.e. $Z=10^{REF(dBZ)/10}$) produced the best results. When included in the regression analysis, the regression coefficient of REF_{-10} was found to be negative and small in magnitude. This reflected that the three isothermal reflectivity parameters are not totally independent, particularly for REF_{-10} which is always sandwiched between REF_0 and REF_{-20}. As such, REF_{-10} is considered redundant and excluded from the final form of the lightning intensity formulae.

Table III – Rules of thumb for specifying the threshold values of radar parameters in lightning initiation nowcast.

Radar Parameter	Minimum Threshold Values	
	Skill Prioritized	Lead-time Prioritized
TOP (km)	7.6 - 10.9	6.5 - 14.6
VIL (mm)	6.0 - 12.8	1.6 - 7.3
REF_0 (dBZ)	41.5 - 51.7	21.4 - 43.5
REF_{-10} (dBZ)	17.3 - 41.9	0.0 - 31.6
REF_{-20} (dBZ)	0.0 - 30.9	0.0 - 26.4
expected CSI (%)	*71 - 83*	33 - 63
expected LeT (min)	*6.8 - 21.6*	24.7 - 31.8

6. PRELIMINARY RESULTS

6.1 *CG Lightning Initiation*

Our test results based on the Testing Data Set of 21 storm cells (10 with CG lightning and 11 without) showed that the highest CSI attained by the candidate threshold sets is 0.83. There are 17 candidates with CSI exceeding 0.7. Amongst these skillful candidates, the average lead time ranges from 7 to 22 minutes.

If early warning rather than forecast skill takes priority, the highest average lead time attained by the candidate threshold sets is 32 minutes. There are 13 choices with average lead time over 25 minutes. Amongst these long-lead candidates, the CSI ranges from 0.3 to 0.6. Table III summarizes the general rules of thumb for setting threshold values prioritized separately for forecast skill and lead time.

6.2 *Cell Lightning Intensity*

For cell lightning intensity nowcast, a multiple linear regression formula in the form of Eq.(2) was obtained with the following coefficients using the Training Data Set:

$$\begin{aligned} b_{\mathrm{TOP}} &= 6.11\times10^{-2} \\ b_{\mathrm{VIL}} &= 2.60\times10^{-2} \\ b_{Z_0} &= 1.15\times10^{-7} \\ b_{Z_{-20}} &= 1.97\times10^{-6} \end{aligned} \qquad (3)$$

The apparent difference in the order of magnitude is due to the change of units from dBZ to Z (see Subsection 5.4) for the isothermal reflectivities. When the predictors are normalized, the resulting regression coefficients, denoted by β, become comparable in magnitude:

$$\begin{aligned} \beta_{\mathrm{TOP}} &= 0.273 \\ \beta_{\mathrm{VIL}} &= 0.387 \\ \beta_{Z_0} &= 0.037 \\ \beta_{Z_{-20}} &= 0.273 \end{aligned} \qquad (4)$$

By applying the above linear regression formulae to the Testing Data Set, predicted cell lightning intensity was obtained and plotted against observation in Fig. 4. It is

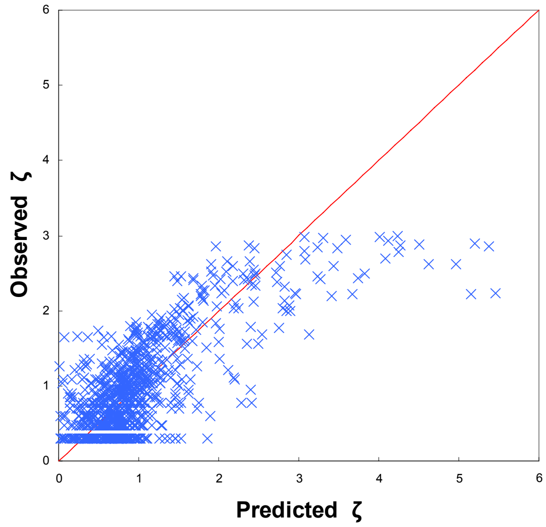

Fig. 4 Observed vs predicted lightning intensity ζ by applying the multiple linear regression formula Eq.(2) to the testing data set.

noted that the predicted intensity aligns with the observations reasonably well for $\zeta < 3$. For predicted intensity beyond 3, it appears that the current multiple regression formulae tends to overpredict. Averaged over all the testing cases, the mean error and root-mean-square error in the predicted ζ are 0.025 and 0.35 respectively.

7. SUMMARY & DISCUSSION

Based on a simple conceptual model of charge separation in a convective cloud, a scheme based on radar reflectivity for the nowcasting of lightning initiation and intensity was developed. Precursors for lightning initiation were identified with radar signatures shown in Table III. Moreover, by taking the logarithm of cell lightning activity as a measure of lightning intensity of a thunderstorm cell, it was found that lightning intensity has an approximate linear relationship with the crucial radar parameters. By making use of model analysis data, isothermal radar reflectivities could be retrieved on a near real-time basis and these parameters were shown to play a significant role in both the initiation and intensity predictions.

The current lightning nowcast study was based on the data sets in 2005. Further studies with more cases spanning the spectrum of thunderstorms will be useful in further enhancing the applicability of the lightning nowcast algorithm.

To improve the robustness of the lightning initiation nowcast algorithm, other independent predictors may also be considered, e.g. cell size and cloud lightning activity. The over-prediction trend seen in the lightning intensity nowcast may not cause problem in practice as long as we limit the predicted intensity to 3 or below. The maximum cell lightning intensity observed in all the training and testing cases is around 3, equivalent to about 1000 CG strokes per 6 min. Considering the spread of the intensity forecast shown in Fig. 4, an alternative approach is to introduce some form of severity index by dividing the lightning intensity scale into broad categories, e.g. severity level I for $\zeta < 1$, level II for $1 \leq \zeta < 2$ and level III for $\zeta \geq 2$.

To put the above lightning nowcast algorithms into operational use, the issue of warning/threat area has to be addressed. This can be estimated by advecting the thunderstorm cells forward in time by the steering flow or the motion vector of individual cell. For this, mean TREC winds (Li and Lai 2004) and G-Track motion vectors can be explored. The problem of warning duration is a more difficult question, requiring knowledge of thunderstorm lifetime.

In terms of warning strategy, the two different sets of threshold values shown in Table III may be used intelligently to set up an effective two-level warning procedure: Level (1) — issue a watch according to the lead-time prioritized threshold values so as to give forecasters early alerts on CG lightning threat; Level (2) — issue the corresponding warning according to the skill-prioritized threshold values so as to enhance POD and reduce FAR as much as possible.

In conclusion, lightning initiation and intensity nowcast algorithms developed in this study are potentially useful for operational use. They will be incorporated into SWIRLS for real-time testing in the rain seasons of 2007.

ACKNOWLEDGEMENT

The authors would like to thank Ms. Hilda Lam for their valuable comments and suggestions.

REFERENCE

Albers, S., J. McGinley, D. Birkenheuer and J. Smart, 1996: The Local Analysis and Prediction System (LAPS): Analyses of clouds, precipitation, and temperature, *Weather and Forecasting*, 11, 273-287.

Byers, H.R. and R.R. Braham, J., 1949: *The Thunderstorm*, U.S. Department of Commerce, pp287.

Jayaratne, R., 2003: Thunderstorm Electrification Mechanisms in V. Cooray (Ed.), *The lightning flash*, The Institution of Electrical Engineers, London, UK, pp17-44.

Cummins, K.L., M.J. Murphy, E.A. Bardo, W.L. Hiscox, R.B. Pyle and A.E. Pifer, 1998: A Combined TOA/MDF Technology Upgrade of the U.S. National Lightning Detection Network, *J. Geophysical Research*, 103, No. D8, 9035-9044.

Dye, J.E., J.J. Jones, W.P. Winn, T.A. Cerni, B. Gardiner, D. Lamb, R.L. Ritter, J. Hallett and C.P.R. Saunders, 1986: Early electrification and precipitation development in a small isolated Montana cumulonimbus, *J. Geophysical Research*, 91, 1231-1247.

Gremillion, M.S. and R. E. Orville, 1999: Thunderstorm Characteristics of Cloud-to-Ground Lightning at the Kennedy Space Center, Florida: A study of Lightning Initiation Signatures as Indicated by the WSR-88D, *Weather and Forecating*, 14, 640-649.

JMA, 2002: Outline of the Operational Numerical Weather Prediction at the Japan Meteorological Agency, Appendix, *WMO Numerical Weather Prediction Progress Report*, 158.

Li, P.W. and E.S.T. Lai, 2004: Short-range quantitative precipitation forecasting in Hong Kong, *J. Hydrology*, 288, 189-209.

Lakshmanan, V. and G.J. Stumpf, 2005: A Real-time Learning Technique to Predict Cloud-to-Ground Lightning, *Joint AMS Fourth Conference on Artificial Intelligence Applications to Environmental Science and 21st International Conference on IIPS for Meteorology, Oceanography, and Hydrology*, San Diego, CA.

Mason, B.J., 1953: A critical examination of theories of charge generation in thunderstorms, *Tellus*, 5, 446-460.

Moore, C.B. and B. Vonnegut, 1977: The thundercloud, in R.H. Golde (Ed.), *Lightning, Vol. 1: Physics of Lightning*, Academic Press, San Diego, CA, pp51-98.

Vaisala, 2004: *IMPACT ESP Model 141-TESP User's Guide Version 1.3*, Vaisala Oyj, Helsinki, Finland.

Williams, E.R., 1985: Large-Scale Charge Separation in Thunderclouds, *J. Geophysical Research*, 90, 6013-6025.

Williams, E.R., 1989: The Tripolar Structure of Thunderstorms, *J. Geophysical Research*, 94, 13151-13166.

Zajac, B.A. and J.F. Weaver, 2002: Lightning Meteorology I: An Introductory Course on Forecasting with Lightning Data, *AMS Interactive Symposium on AWIPS*, Orlando, FL, USA.